ACS OMEGA

Open Access

http://pubs.acs.org/journal/acsodf

Article

Enhanced Bioadhesive and Antimicrobial Properties of PVA/Ascorbic Acid Composite with Tannic Acid Synthesized by Gamma Irradiation for Biomedical Applications

Shreen Adel Rashiq, Nour E. A. Abd El-Sattar, Hoda Abd Elhay abd Elhamid, Gharieb S. El-Sayyad, Ghada Bassioni, and Mohamed Mohamady Ghobashy*

Cite This: *ACS Omega* 2025, 10, 13839−13853

Read Online

ACCESS | Metrics & More | Article Recommendations

ABSTRACT: Bioadhesive hydrogels play a crucial role in biomedical applications due to their capacity to adhere to biological surfaces. This study investigates a novel bioadhesive hydrogel system developed from poly(vinyl alcohol) (PVA) and ascorbic acid (AS), cross-linked through gamma irradiation at 7 kGy, and modified with 5 wt % tannic acid (TA). The primary objective was to enhance the hydrogel's bioadhesive, mechanical, and antimicrobial properties. Mechanical testing revealed that the (PVA/AS)/TA hydrogel exhibited significant improvements, with a lap shear strength of 92 kPa, a tensile strength of 0.57 MPa, and an elongation at break of 180%, compared to the unmodified variant. Antimicrobial efficacy was assessed against bacterial strains, including *Staphylococcus aureus* and *Escherichia coli*, showing potent inhibitory effects with minimum inhibitory concentration (MIC) values of 25 μg/mL and 30 μg/mL, respectively. The findings indicate that the (PVA/AS)/TA hydrogel is a promising candidate for wound healing, drug delivery, and tissue engineering applications. It showcases its novelty in improving bioadhesive properties while providing antimicrobial functionality, thus addressing critical challenges in biomedical material design.

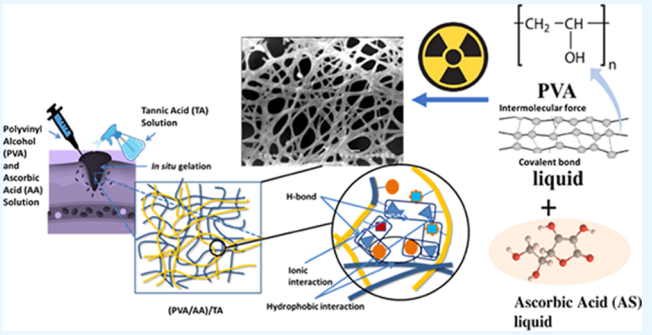

1. INTRODUCTION

Bioadhesive hydrogels have garnered significant attention in biomedical applications due to their ability to adhere to biological surfaces and provide sustained delivery of therapeutic agents. These versatile materials represent a promising frontier in developing advanced drug delivery systems, tissue engineering scaffolds, and wound healing technologies.[1] By combining the properties of hydrogels highly hydrated, three-dimensional polymer networks with bioadhesive characteristics, researchers have created a class of biomaterials that can intimately interact with biological tissues while maintaining their structural integrity and functionality.[2]

Recent research has highlighted significant findings in application of advanced material.[3,4] Complemented by explored innovative hydrogel for environmental application[5−8] One of the key advantages of bioadhesive hydrogels is their ability to provide sustained and controlled release of therapeutic agents. Researchers can achieve prolonged release profiles that maintain therapeutic concentrations over extended periods by incorporating drugs or bioactive molecules within the hydrogel network.[9] This characteristic is precious in the treatment of chronic conditions or in situations where frequent drug administration is impractical or undesirable. Furthermore, the intimate contact between the bioadhesive hydrogel and the target tissue can enhance local drug concentrations,[10] potentially reducing systemic side effects and improving overall treatment efficacy. Developing bioadhesive hydrogels involves carefully considering various factors, including polymer composition, cross-linking density, and incorporating specific functional groups that promote adhesion to biological surfaces.[11] Common polymers used in the fabrication of bioadhesive hydrogels include natural polymers such as chitosan, alginate, and hyaluronic acid, as well as synthetic polymers like poly(acrylic acid), poly(vinyl alcohol), and poly(ethylene glycol).[12] These polymers can be modified or combined to achieve desired mechanical properties, swelling behavior, and bioadhesive strength. The application of bioadhesive hydrogels extends beyond traditional drug delivery systems. In tissue engineering, these materials serve as scaffolds supporting cell growth,[1] promoting

Received: August 2, 2024
Revised: December 4, 2024
Accepted: December 6, 2024
Published: April 3, 2025

tissue regeneration, and facilitating the controlled release of growth factors or other bioactive molecules. Bioadhesive hydrogels have shown promise in the engineering of soft tissues, such as cartilage and skin, where their ability to mimic the extracellular matrix and provide a supportive environment for cell proliferation and differentiation is highly advantageous. Despite bioadhesive hydrogels' numerous advantages and potential applications, several challenges remain in their development and clinical translation.[13] One of the primary challenges is achieving an optimal balance between bioadhesion strength and the ability of the hydrogel to maintain its structural integrity over time. Hydrogels that adhere too strongly to biological surfaces may cause tissue damage upon removal, while those with insufficient adhesion may not provide the desired therapeutic effects. Researchers are exploring various strategies to address this challenge, including developing mucoadhesive polymers with reversible bonding mechanisms and incorporating enzymatically degradable cross-links.[14]

The mechanical properties of bioadhesive hydrogels also play a crucial role in their performance and applicability. Depending on the intended application, hydrogels may need to withstand various mechanical stresses while maintaining their structural integrity and bioadhesive properties.[15] The current article explores various strategies to enhance the mechanical strength of bioadhesive hydrogels, including the incorporation of nanoparticles, the development of double-network hydrogels, and the use of novel cross-linking techniques. Including tannic acid (TA) in poly(vinyl alcohol) (PVA)/ascorbic acid (AA) blend solutions is a strategic approach to facilitate the formation of a robust bioadhesive hydrogel through various intermolecular interactions. TA, a polyphenolic compound with diverse functional groups, can interact with both PVA and AA via hydrogen bonding, ionic bonding, and hydrophobic interactions.[16] These interactions contribute significantly to the hydrogel network's self-assembly and cross-linking. TA possesses numerous phenolic and carbonyl groups that can act as both hydrogen bond donors and acceptors. PVA, a synthetic polymer with hydroxyl groups, can form hydrogen bonds with TA's phenolic and carbonyl groups.

The incorporation of tannic acid into poly(vinyl alcohol) (PVA) hydrogels enhances their bioadhesive properties, enabling strong adhesion to biological tissues, which is essential for applications like wound dressings requiring prolonged tissue contact.[17] Additionally, the PVA/tannic acid (TA) composite hydrogels exhibit significant antimicrobial activity, making them effective against various pathogens, which is crucial for preventing infections in wound care applications.[18] The mechanical properties of these hydrogels can be optimized by adjusting tannic acid concentrations and the irradiation doses used during preparation. Studies indicate that the resulting hydrogels exhibit high tensile strength and elasticity, which are particularly important for use in dynamic biological environments. Furthermore, these hydrogels demonstrate excellent biocompatibility, making them suitable for a range of medical applications, including wound healing and tissue engineering.[19] Similarly, AA, with its carboxyl and hydroxyl groups, can participate in hydrogen bonding interactions with TA.[16] These hydrogen bonding interactions contribute to the physical cross-linking and self-assembly of the (PVA/AS)/TA hydrogel system. The formation of a network of hydrogen bonds enhances the hydrogel's structural integrity and contributes to its mechanical strength. While significant progress has been made in bioadhesive hydrogels, several areas require further investigation to fully realize their potential in biomedical applications.[20] One such area is developing improved in vitro models and better testing methods to predict these materials' in vivo performance. Current methods for assessing bioadhesion strength and drug release profiles often rely on simplified models that may not accurately reflect biological tissues' complex and dynamic environment. Developing more sophisticated, physiologically relevant testing platforms could accelerate the translation of novel bioadhesive hydrogel formulations from the laboratory to clinical applications.[21] This research aims to develop a multifunctional bioadhesive hydrogel with enhanced mechanical and antimicrobial properties suitable for various biomedical applications. The novelty lies in the unique combination of PVA and ascorbic acid, cross-linked via gamma irradiation and modified with tannic acid.

Gamma irradiation induces cross-linking in PVA chains, enhancing the mechanical strength and elasticity of the hydrogels. This cross-linking results from the generation of free radicals by γ rays, facilitating the formation of covalent bonds between polymer chains and forming a more stable and robust network.[22] The increased cross-link density also improves adhesion properties, as a stronger matrix can interact more effectively with biological tissues. The presence of tannic acid enhances hydrogen bonding interactions between PVA and tannic acid molecules, and gamma irradiation further promotes these interactions by modifying the functional groups within the polymer matrix, resulting in a more cohesive structure.[23]

The research addresses key challenges in hydrogel development, such as achieving an optimal balance between adhesion and mechanical strength. It provides a comprehensive analysis of the hydrogel's properties, paving the way for its application in wound healing, drug delivery, and tissue engineering. The novelty of this research lies in the unique formulation of a bioadhesive hydrogel composed of poly(vinyl alcohol) (PVA) and ascorbic acid (AA), cross-linked via gamma irradiation and modified with tannic acid (TA). This approach synergistically enhances the hydrogel's mechanical and antimicrobial properties, addressing key challenges in hydrogel development. The resulting (PVA/AS)/TA hydrogel shows significant promise for wound healing, drug delivery, and tissue engineering applications.

2. EXPERIMENTAL SECTION

2.1. Materials. Poly(vinyl alcohol) (PVA) and ascorbic acid (AS) were the main components for preparing the bioadhesive hydrogel formulations. PVA, with an average molecular weight of 88.000 and a degree of hydrolysis of 21%, was obtained from Sigma-Aldrich Co., while AS, with a purity of 98%, was purchased from Acros.

2.2. Preparation of PVA/AS Hydrogels by Gamma Irradiation. The gamma irradiation technique synthesized the PVA/AS hydrogel formulations using a ^{60}Co gamma source. The required amounts of PVA and AS were accurately weighed and dissolved in distilled water to obtain a 10% w/v PVA solution with varying AS concentrations of 0%, 1%, 2%, 3%, 4%, and 5% w/w concerning PVA. The solutions were thoroughly mixed until a homogeneous mixture was obtained. The homogeneous PVA/AS solutions were poured into specialized containers suitable for gamma irradiation and sealed to prevent evaporation. The sealed containers were then

https://doi.org/10.1021/acsomega.4c07119
ACS Omega 2025, 10, 13839−13853

subjected to gamma irradiation at different doses of 0, 3, 7, 9, 12, and 15 kGy using a gamma irradiator [The irradiation technique was carried out by a Gamma Cell (^{60}Co source) irradiation unit Model 220 located at National Center for Radiation Research and Technology (NCRRT). At the time of the experimental research, the dose rate was 1.107 kGy/hour]. After irradiation, the PVA/AS blend formulations were carefully kept at a temperature of 4 °C with a relative humidity (RH%) of 50% for further characterization and analysis. The compositions of the various PVA/AS blend formulations irradiated by gamma irradiation, along with their respective codes, are summarized in Table 1.

Table 1. Compositions of PVA/Ascorbic Acid (PVA/AS) Blends Prepared via Gamma Irradiation with Varying Ascorbic Acid Concentrations and Irradiation Doses

Samples/contents	PVA	Ascorbic acid	Dose (kGy)	Key
1	10%	0%	0	$(P_{10}A_0)_{0k}$
2	10%	0%	3	$(P_{10}A_0)_{3k}$
3	10%	0%	7	$(P_{10}A_0)_{7k}$
4	10%	0%	9	$(P_{10}A_0)_{9k}$
5	10%	0%	12	$(P_{10}A_0)_{12k}$
6	10%	0%	15	$(P_{10}A_0)_{15k}$
7	10%	1%	0	$(P_{10}A_1)_{0k}$
8	10%	1%	3	$(P_{10}A_1)_{3k}$
9	10%	1%	7	$(P_{10}A_1)_{7k}$
10	10%	1%	9	$(P_{10}A_1)_{9k}$
11	10%	1%	12	$(P_{10}A_1)_{12k}$
12	10%	1%	15	$(P_{10}A_1)_{15k}$
13	10%	2%	0	$(P_{10}A_2)_{0k}$
14	10%	2%	3	$(P_{10}A_2)_{3k}$
15	10%	2%	7	$(P_{10}A_2)_{7k}$
16	10%	2%	9	$(P_{10}A_2)_{9k}$
17	10%	2%	12	$(P_{10}A_2)_{12k}$
18	10%	2%	15	$(P_{10}A_2)_{15k}$
19	10%	3%	0	$(P_{10}A_3)_{0k}$
20	10%	3%	3	$(P_{10}A_3)_{3k}$
21	10%	3%	7	$(P_{10}A_3)_{7k}$
22	10%	3%	9	$(P_{10}A_3)_{9k}$
23	10%	3%	12	$(P_{10}A_3)_{12k}$
24	10%	3%	15	$(P_{10}A_3)_{15k}$
25	10%	4%	0	$(P_{10}A_4)_{0k}$
26	10%	4%	3	$(P_{10}A_4)_{3k}$
27	10%	4%	7	$(P_{10}A_4)_{7k}$
28	10%	4%	9	$(P_{10}A_4)_{9k}$
29	10%	4%	12	$(P_{10}A_4)_{12k}$
30	10%	4%	15	$(P_{10}A_4)_{15k}$
31	10%	5%	0	$(P_{10}A_5)_{0k}$
32	10%	5%	3	$(P_{10}A_5)_{3k}$
33	10%	5%	7	$(P_{10}A_5)_{7k}$
34	10%	5%	9	$(P_{10}A_5)_{9k}$
35	10%	5%	12	$(P_{10}A_5)_{12k}$
36	10%	5%	15	$(P_{10}A_5)_{15k}$

Scheme 1 address the possible preparation mechanism of the blend. Initially, the components consist of poly(vinyl alcohol) (PVA) in liquid form, ascorbic acid (AS) in liquid form, and tannic acid. The first step involves combining PVA and ascorbic acid solutions, which creates an initial network through hydrogen bonding and possible physical entanglements. Subsequently, the mixture is exposed to γ radiation, initiating radical formation, likely primarily from ascorbic acid.

Scheme 1. Represent of the Synthesis Process for PVA/AS/TA Bioadhesive Hydrogel.[a]

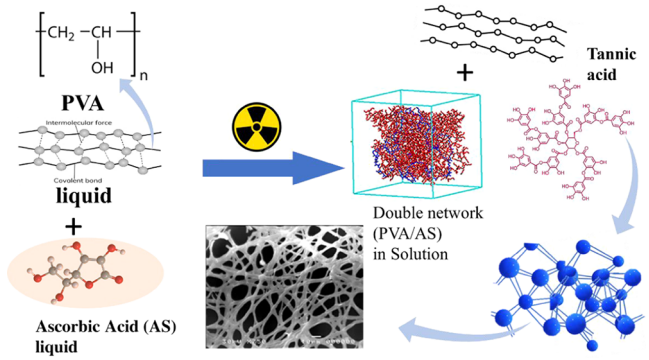

[a]The process involves mixing poly(vinyl alcohol) (PVA) and ascorbic acid (AS) solutions, followed by gamma irradiation to form a double network structure. Tannic acid (TA) is subsequently incorporated, resulting in a complex hydrogel with fibrous morphology as evidenced by SEM imaging.

This irradiation process promotes cross-linking between PVA chains, with ascorbic acid potentially acting as a cross-linking agent or radical initiator, resulting in the formation of a "double network" structure. After irradiation, tannic acid is incorporated into the mixture, where it likely interacts through hydrogen bonding with both PVA and ascorbic acid, further reinforcing the network structure. This combination of covalent cross-links (formed during irradiation) and non-covalent interactions (hydrogen bonding) leads to the formation of a robust three-dimensional network, contributing to the fibrous structure observed in the SEM image. The proposed mechanism highlights the role of each component in network formation, detailing how gamma irradiation promotes covalent bond formation and how the interactions, covalent bonds, hydrogen bonds, and physical entanglements collectively contribute to the unique properties of the final hydrogel. This mechanism effectively explains the transition from the initial individual components to the formation of a complex "double network" structure, incorporating the effects of irradiation and the distinct roles of PVA, ascorbic acid, and tannic acid in enhancing the properties of the resulting hydrogel.

2.3. Antimicrobial Activity. Antimicrobial activity of (P10A2)7k/TA (250 μg/mL) was evaluated toward *Pseudomonas aeruginosa*, *Klebsiella pneumoniae* and *Escherichia coli* as a model of Gram-negative bacteria while *Staphylococcus aureus*, *Staphylococcus epidermidis* and *Bacillus subtilis* as a model of Gram-positive bacteria in addition to *Candida albicans* and *Candida tropicalis as unicellular organisms*. The tested microbes were known to cause wound infection according to the culture collection of Drug Microbiology Lab., Drug Radiation Research Department, EAEA, Cairo, Egypt. The agar well distribution procedure strictly followed CLSI guideline M51-A2.[24]

Placing 100 μL of (P10A2)7k/TA (250 μg/mL), DMSO, and standard antibiotic (Clindamycin (DA); 2 μg/mL), and antifungal drug Nystatin (NS, 100 μg/mL) in agar wells (7 mm) seeded with bacterial and fungal strains separately. Then incubating at 37 °C for 24−48 h, inhibition zones were measured, and MIC was determined using the microdilution method.[25] *Candida* species were retained at 2−4 × 10^7 CFU/

https://doi.org/10.1021/acsomega.4c07119
ACS Omega 2025, 10, 13839−13853

Table 2. Viscosity Data for PVA/AS Blends

Viscosity (cP)	172400	607	667	646	761	693
AA content	$(P_{10}A_0)_{7k}$	$(P_{10}A_1)_{7k}$	$(P_{10}A_2)_{7k}$	$(P_{10}A_3)_{7k}$	$(P_{10}A_4)_{7k}$	$(P_{10}A_5)_{7k}$

mL, while bacterial inoculums were created at 3−6 × 10^7 CFU/mL.

2.4. Antibiofilm Potential of the Prepared (P10A2)7k/TA. A qualitative estimation of biofilm formation was studied according to Christensen et al.[26] Investigated was the visual examination of the biofilm formed at the tube wall with and without (P10A2)7k/TA, (250 μg/mL) were tested for their ability to inhibit the growth of sensitive bacteria compared to the control sample.

After adjusting at 0.5 McFarland, approximately 5.0 mL of nutrient-rich broth was added to each tube, and the broth, including the investigated bacteria and unicellular microbes, was treated. Subsequently, the resulting solution was incubated at 37.0 ± 2 °C for an entire night. After carefully removing the tubes' contents, they were cleaned with PBS (pH 7) and dried.[27] The attached bacterial layers were washed with deionized water after being fixed with 3.0% sodium acetate for 10 min. Bacterial biofilms were stained with 0.1% crystal violet (CV) for 15.0 min, and any leftover stain was removed with deionized water. Ultimately, 3.0 mL of ethanol was combined to separate the stain. A UV−vis spectrometer (at 570.0 nm) was used to analyze the microbial biofilms. Equation 1 was used to calculate the inhibition percentage.

$$R\% = 100 \times (\text{O.D. of control sample} - \text{O.D. of the treated sample}) / (\text{O.D. of control sample}) \quad (1)$$

2.5. Growth Curve Assay. The influence of the synthesized (P10A2)7k/TA (250 μg/mL) on the growth of *S. aureus*, and *E. coli* (the most sensitive microbes) was determined by the growth curve assay according to Huang et al.[28] The microbial suspension was adapted to 0.5 McFarland (1 × 10^8 CFU/mL) in 5.0 mL of nutrient broth tubes. (P10A2)7k/TA were included separately in the examined tubes. The absorbance of the microbial growth following treatment was evaluated each 2 h intervals up to 24 h. (wavelength of 600 nm). The relationship was conducted between the average number of duplicate readings and the time required to obtain the typical growth curve.

2.6. Effect of (P10A2)7k/TA on Protein Leakage from Bacterial Cell Membranes. A 0.5 McFarland (1 × 10^8 CFU/mL) pure 18-h bacterial culture was set, and 100 μL was injected into 10 mL of the nutritional broth that included scattered and well-sonicated (P10A2)7k/TA at different concentrations (0.125, 0.25, 0.5, and 1.0 mg/mL). The control was a broth infused with culture but did not include (P10A2)7k/TA. After 5 h of incubation at 37 °C, all treated samples were centrifuged for 15 min at 5500 rpm.[29] 1 mL of Bradford reagent was mixed with 100 μL of supernatant for each sample. The optical density was determined after 10 min of dark incubation at 595 nm.[29]

2.7. Statistical Analysis. A one-way ANOVA To statistically analyze the options at $p = 0.05$, Duncan's different areas and the least significant difference (LSD) analysis were utilized.[30] The statistical program SPSS (version 15) analyzed and evaluated information and results.

3. RESULTS AND DISCUSSION

3.1. The Effect of Ascorbic Acid Content on Viscosity of PVA/AS Blends. The viscosity of polymer solutions is a fundamental parameter that significantly influences their processing, handling, and application properties. This parameter is particularly crucial in bioadhesive hydrogels, where viscosity impacts adhesive strength, spreadability, and retention at the application site. Table 2 and Figure 1 present the viscosity data for poly(vinyl alcohol) (PVA) and ascorbic acid (AA) blends that were irradiated at a dose of 7 kGy, with varying concentrations of AA ranging from 0% to 5% w/w concerning PVA. The data shows that the viscosity of the PVA/AS blends decreases as the concentration of ascorbic acid increases. Specifically, the sample with 0% AA (P10A0)7k exhibits the highest viscosity of 172400 cP, whereas the sample with 5% AA (P10A1)7k shows the lowest viscosity at 607 cP. The observed decrease in viscosity with increasing AA concentration can be attributed to several factors. First, ascorbic acid is a small molecular weight compound that acts as a viscosity reducer or thinning agent when added to the PVA solution. The presence of AA disrupts the intermolecular hydrogen bonding between PVA chains, reducing the blend's overall viscosity. This disruption results in a more fluid and less viscous solution, as the polymer chains are less entangled and can move more freely.

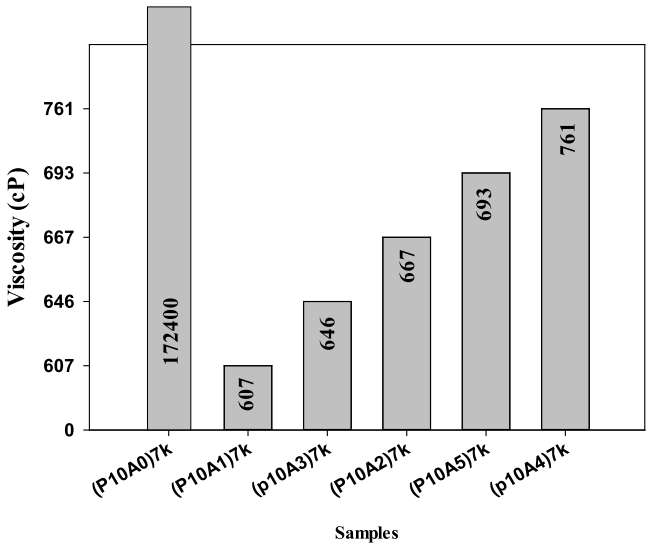

Figure 1. Viscosity of PVA/AS blends with varying ascorbic acid concentrations.

Second, the addition of AA increases the ionic strength of the solution. This increase in ionic strength can cause the PVA chains to adopt a more compact conformation due to charge screening effects. The compacted chains reduce the polymer chain extension and entanglement, further contributing to the decrease in viscosity. The ability of AA to influence the ionic environment within the solution highlights its role in modifying the physical properties of the polymer matrix.

Another significant factor is AA's potential to facilitate free radical formation during gamma irradiation. Free radicals can

https://doi.org/10.1021/acsomega.4c07119
ACS Omega 2025, 10, 13839−13853

Table 3. Viscosity Data for PVA/AS Blends with Varying Irradiation Doses

Viscosity (cP)	582	767	667	620	743	719
Dose	$(P_{10}A_2)_{0k}$	$(P_{10}A_2)_{3k}$	$(P_{10}A_2)_{7k}$	$(P_{10}A_2)_{9k}$	$(P_{10}A_2)_{12k}$	$(P_{10}A_2)_{15k}$

induce chain scission or degradation of PVA chains, leading to shorter polymer chains that exhibit lower viscosities than their longer counterparts. The degradation process results in a decrease in molecular weight and, consequently, a reduction in viscosity. This mechanism underscores the impact of gamma irradiation and AA on the molecular structure of the polymer blend.

Additionally, the presence of AA may influence the degree of cross-linking or network formation within the PVA hydrogel during gamma irradiation. Lower cross-linking densities can decrease viscosities as the polymer network becomes less dense and more flexible. The interaction between AA and the cross-linking process is crucial for understanding the rheological behavior of the hydrogel under different conditions.

From a practical standpoint, the ability to modulate the viscosity of bioadhesive hydrogels by varying the AA content is advantageous. Higher viscosities may be desirable for applications requiring better retention and adhesion at the application site, ensuring that the hydrogel remains in place as biomaterials. In contrast, lower viscosities could facilitate easier handling, spreading, and injection of the hydrogel formulations, making them more suitable for applications where precise application and ease of use are critical.

3.2. The Effect of Irradiation Dose on Viscosity of PVA/AS Blends. viscosity changes in PVA/AS blends under gamma irradiation provide crucial insights into how irradiation dose can modulate polymer solution properties. Understanding these factors enables researchers and developers to design bioadhesive hydrogels with optimized performance for targeted medical applications. The data presented in Table 3 and visualized in Figure 2 offers a quantitative basis for predicting

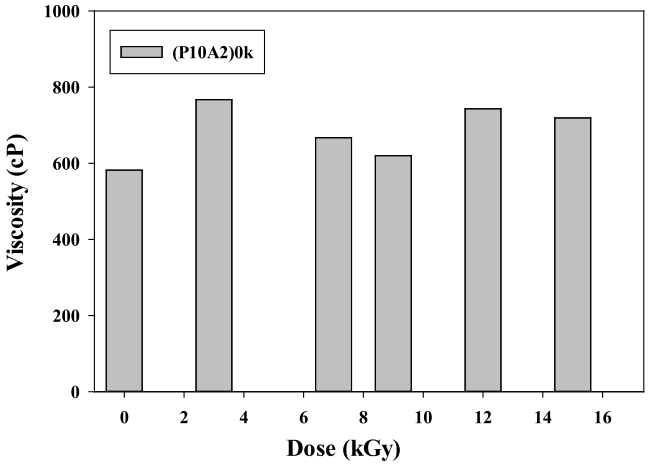

Figure 2. Effect of Irradiation Dose on Viscosity of PVA/AS Blends.

hydrogel behavior under various irradiation conditions, essential for optimizing the balance between viscosity, cross-linking, and mechanical properties in biomedical applications. Table 3 and Figure 2 present the viscosity data for the PVA/AS blends containing 2% ascorbic acid (AA) subjected to different gamma irradiation doses ranging from 0 kGy (nonirradiated) to 15 kGy. The data shows that the viscosity of the PVA/AS blends generally increases with increasing irradiation dose, with some exceptions at lower doses. The nonirradiated sample (P10A2)0k exhibits a relatively low viscosity of 582 cP, which can be attributed to the absence of cross-linking and the presence of linear or minimally branched PVA chains. As the irradiation dose increases, the viscosity remains unchanged (at 3 kGy) or decreases slightly (at 7 kGy). This behavior could be attributed to the following factors: (1) At lower irradiation doses, the predominant effect is the formation of free radicals, which can lead to chain scission or degradation of PVA chains, resulting in a temporary decrease in viscosity. (2) The presence of ascorbic acid (AA) may also contribute to the initial viscosity decrease by facilitating free radical formation and PVA chain scission at lower doses. (3) However, as the irradiation dose increases further (beyond 7 kGy), a significant increase in viscosity is observed, with the highest viscosity of 743 cP achieved at 12 kGy. This viscosity increase can be attributed to the following factors: (1) At higher irradiation doses, the cross-linking of PVA chains becomes the dominant process, forming a three-dimensional network structure. This cross-linking increases the molecular weight and entanglement of the polymer chains, resulting in higher viscosities. (2) The presence of ascorbic acid (AA) may contribute to the cross-linking process by generating free radicals and facilitating the formation of intermolecular and intramolecular cross-links between PVA chains. (3) The increased cross-linking density at higher irradiation doses also restricts the mobility and flexibility of the polymer chains, further contributing to the observed viscosity increase. It is worth noting that at the highest irradiation dose of 15 kGy, a slight decrease in viscosity (719 cP) is observed compared to the 12 kGy sample. This behavior could be attributed to potential chain scission or degradation processes occurring at very high irradiation doses, which may outweigh the cross-linking effects, leading to a slight viscosity reduction. The ability to modulate the viscosity of PVA/AS hydrogel formulations by varying the irradiation dose is advantageous for tailoring the rheological properties to suit specific biomedical applications. Higher viscosities may be desirable for applications requiring better retention and adhesion, while lower viscosities could facilitate easier handling, spreading, and injection of the hydrogel formulations. It is important to consider the viscosity data in conjunction with other properties, such as bioadhesive strength, swelling behavior, and degradation profiles, to optimize the formulation for the desired application.

3.3. Adhesion Strength-Based, Adding Tannic Acid (TA) to the PVA/AS Blend Solution to Form Bioadhesive Materials. The mechanical properties of (PVA/AS)/TA hydrogels prepared via gamma irradiation, as presented in Table 4, offer valuable insights into these materials' performance and potential applications. The comprehensive data, encompassing lap shear strength, tensile strength, elongation at break, and Young's modulus for various hydrogel formulations with different TA content and irradiation doses, provides a robust foundation for evaluating the hydrogels' suitability for diverse biomedical applications. Lap shear strength, a critical indicator of the hydrogel's adhesive capabilities, demonstrates a notable trend with increasing TA content. The data reveals that adhesive strength improves as TA concentration rises,

https://doi.org/10.1021/acsomega.4c07119
ACS Omega 2025, 10, 13839−13853

Table 4. Mechanical Properties of (PVA/AS)/TA Hydrogels

	(P10A2) 7k + 1 wt % TA	(P10A2) 7k + 3 wt % TA	(P10A2) 7k + 5 wt % TA	(P10A2) 7k + 7 wt % TA	(P10A2) 7k + 10 wt % TA
lap shear strength (kPa)	45	55	70	92	80
tensile strength (MPa)	0.28	0.35	0.42	0.57	0.48
elongation at break (%)	120	140	165	180	170
Young's modulus (MPa)	0.45	0.52	0.68	0.85	0.72

reaching a peak of 92 kPa for the formulation containing 7 wt % TA. This optimal point suggests a synergistic interaction between the PVA/AS matrix and the TA component, likely due to enhanced cross-linking and intermolecular interactions. However, the slight decrease in lap shear strength observed at 10 wt % TA indicates a threshold beyond which additional TA may not improve adhesion. This behavior could be attributed to the oversaturation of cross-linking sites or potential interference with the polymer network structure at higher TA concentrations.

The tensile strength and elongation at break data provide crucial information about the hydrogel's mechanical integrity and flexibility. Both properties show a positive correlation with TA content, culminating in maximum values of 0.57 MPa for tensile strength and 180% for elongation at break in the formulation with 7 wt % TA. This simultaneous improvement in strength and flexibility is particularly noteworthy, as it suggests that incorporating TA enhances the hydrogel's overall mechanical performance without compromising its elasticity. Such a combination of properties is highly desirable in biomedical applications where the material must withstand mechanical stresses while maintaining flexibility to conform to biological tissues or interfaces. Young's modulus data further complements the mechanical property profile, offering insights into the hydrogel's stiffness and elasticity. The observed increase in Young's modulus with TA content, peaking at 0.85 MPa for the 7 wt % TA formulation, indicates a progressive enhancement in the material's structural rigidity. This trend aligns with the improvements in tensile strength, suggesting that TA incorporation strengthens the hydrogel network and increases its resistance to deformation under stress. The ability to modulate the Young's modulus is particularly valuable in tissue engineering applications, where matching the mechanical properties of the scaffold to those of the target tissue is crucial for proper cell growth and differentiation. The interplay between these mechanical properties and their dependence on TA content and irradiation dose highlights the versatility of these hydrogel systems. By adjusting these parameters, researchers can fine-tune the hydrogel's characteristics to meet specific requirements for various biomedical applications. For instance, formulations with higher lap shear strength could be ideal for wound dressings or surgical adhesives, where strong adhesion to biological tissues is paramount.

Conversely, hydrogels with optimized tensile strength and elongation at break might be more suitable for applications involving dynamic mechanical environments, such as cartilage or tendon repair, where the material must withstand repeated deformation cycles. Moreover, controlling Young's modulus opens up possibilities in tissue engineering and regenerative medicine. By matching the stiffness of the hydrogel to that of the target tissue, researchers can create more biomimetic scaffolds that promote appropriate cell behavior and tissue development. This control over mechanical properties is precious in applications targeting tissues with varying mechanical requirements, from soft tissues like skin to more rigid structures like bone. The comprehensive data in Table 4 allow a nuanced understanding of how TA content and irradiation dose influence the hydrogel's mechanical behavior. This wealth of information enables researchers to make

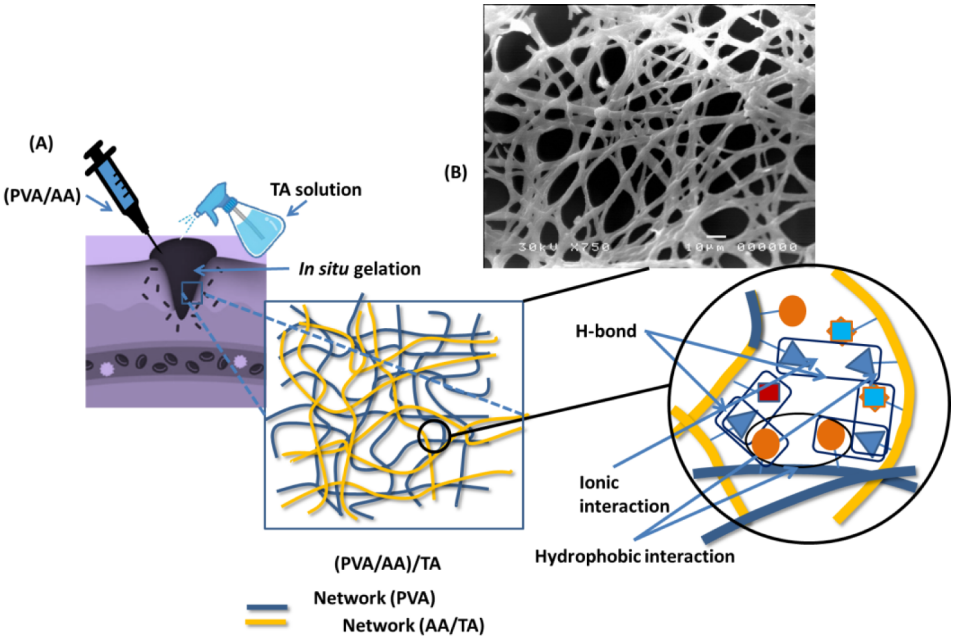

Figure 3. Schematic illustration of the fabrication process and mechanisms of bioadhesion. (A) Schematic illustrating the fabrication process and putative cross-linked structure of (PVA/AS)/TA hydrogels. (B) SEM image analysis of (PVA/AS)/TA hydrogels.

https://doi.org/10.1021/acsomega.4c07119
ACS Omega 2025, 10, 13839−13853

informed decisions when designing hydrogels for specific biomedical applications, balancing factors such as adhesion strength, mechanical integrity, flexibility, and structural support.

3.4. Fast Gelation and Fibril Structure of PVA/AS/TA Bioadhesive Hydrogels. The ultrafast gelation of the PVA/AS/TA bioadhesive hydrogel at ambient temperature is a significant advantage, as it allows easy application and conformation to the target tissue surface. The ability to form the hydrogel by simply mixing the polymer precursor solution (P10A2)7k with the TA solution highlights the simplicity and practicality of the system. The strong adhesion and retention of the PVA/AS/TA bioadhesive hydrogel on wet tissue surfaces, as shown in Figure 3A, is a crucial feature for biomedical applications. This bioadhesive property enables the hydrogel to remain in close contact with the target site, facilitating sustained drug delivery and wound healing. The SEM image of the PVA/AS/TA bioadhesive hydrogel (Figure 3B) reveals a fibrillar morphology. This fibrillar structure enhances the surface area and porosity of the hydrogel, potentially improving drug penetration and oxygen permeability. The increased oxygen permeability can promote faster wound healing, making the PVA/AS/TA bioadhesive hydrogel a promising candidate for wound dressing applications.

Furthermore, the bioadhesive properties of the PVA/AS/TA hydrogel make it suitable for applications in promoting gastrointestinal (GI) mucosal healing. The ability to adhere to the mucosal surfaces can facilitate localized drug delivery, protect the affected areas, and support the healing process. Overall, the ultrafast gelation, strong bioadhesive properties, fibrillar morphology, and potential for improved drug penetration and oxygen permeability make the PVA/AS/TA bioadhesive hydrogel a promising biomaterial for various biomedical applications, including wound healing, drug delivery, and gastrointestinal mucosal healing.

3.5. The TEM and SEM Analysis of (PVA/AS) and (PVA/AS)/TA. The TEM images in Figure 4 illustrate the nanostructure of poly (vinyl alcohol) (PVA) with ascorbic acid that has undergone irradiation at 7 kGy (P10A2)7k. Image (a) provides a lower magnification view of the material, revealing a larger structure with irregular edges, and highlights a specific area with a white rectangular box for further examination. Figure 4b shows a grainy texture along the material's edge, highlighting a region of interest with two molecules to form a spherical shape. Figure 4b–d provides an even higher magnification, focusing on the material's detailed, clustered structure. It shows a densely packed collection of small particles or granules, offering the finest structural details that provide insights into the irradiated material's morphology. Figure 4e is a scanning electron microscopy (SEM) image of the (PVA/AS)/TA composite material, specifically the (P10A2)7k sample. This SEM image was taken at 200× magnification. It provided detailed insights into the morphology of the composite material, highlighting its interconnected network with a fibrous. The visible pores and the fibrous network suggest that the composite material may have a significant surface area. The presence of irregular fragments and sheet-like structures indicates regions where components of the composite may have aggregated or where interactions between PVA, AS, and TA have resulted in phase changes during sample preparation.

3.6. FTIR Analysis of (PVA/AS)/TA Sample. Figure 5a presents the FTIR spectrum of tannic acid, revealing

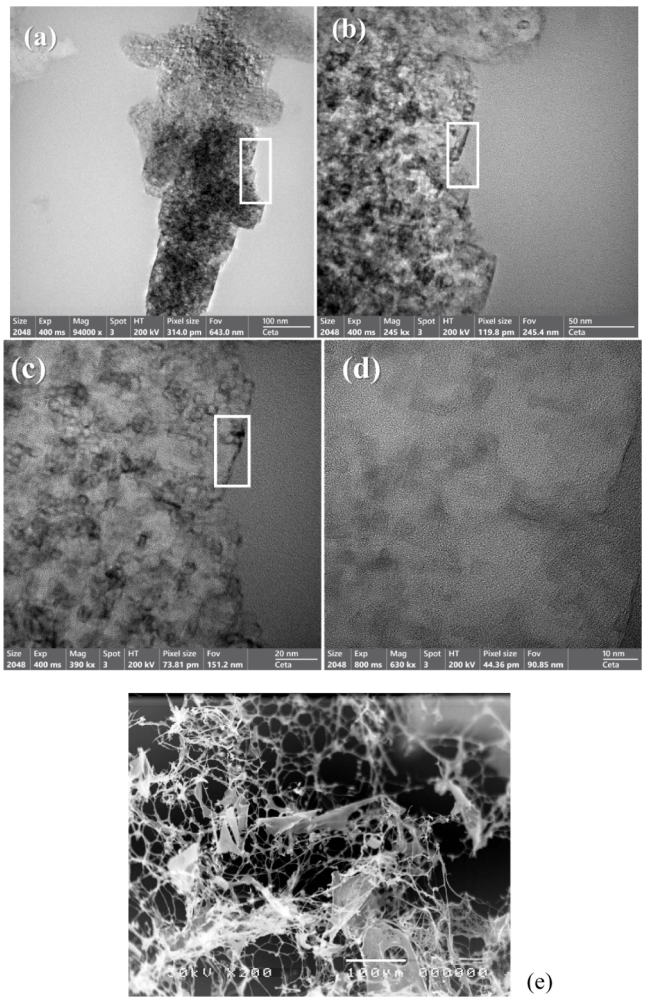

Figure 4. (a–d) TEM image of (PVA/AS) and (e) SEM image of (PVA/AS)/TA.

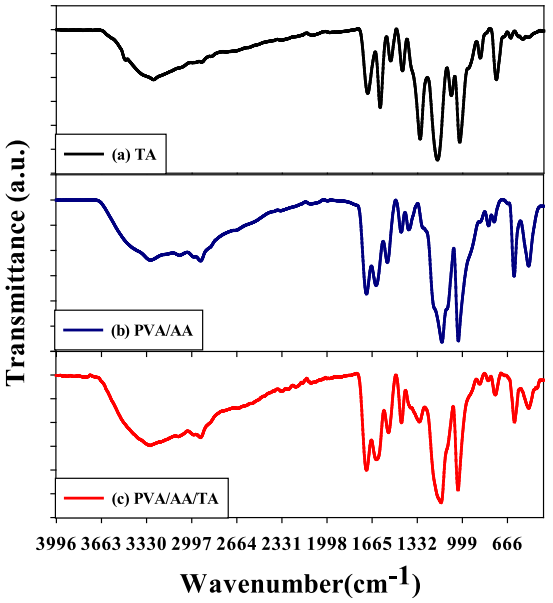

Figure 5. the FTIR of (a) tannic acid, (b) PVA/ascorbic acid and (c) PVA/tannic acid/ascorbic acid.

https://doi.org/10.1021/acsomega.4c07119
ACS Omega 2025, 10, 13839−13853

Table 5. Water Evaporation for PVA/AS Blends

sample time	$(P_{10}A_0)_{7k}$	$(P_{10}A_1)_{7k}$	$(P_{10}A_2)_{7k}$	$(P_{10}A_3)_{7k}$	$(P_{10}A_4)_{7k}$	$(P_{10}A_5)_{7k}$
0.5	16.67%	0%	3.57%	0%	0%	1.96%
1	27.92%	0%	10.71%	12.5%	10%	7.84%
2	41.25%	25%	17.86%	37.5%	10%	13.73%
3	52.92%	25%	25.00%	37.5%	20%	17.65%
4	56.25%	25%	28.57%	37.5%	30%	21.57%
8	81.25%	100%	93.21%	37.5%	40%	23.53%
13	88.33%	100%	35.71%	50%	50%	25.49%
16	89.58%	100%	42.86%	50%	50%	35.29%
21	92.50%	100%	42.86%	50%	50%	37.25%
24	93.33%	100%	46.43%	50%	50%	35.29%
52	94.58%	100%	46.43%	50%	50%	47.06%

characteristic peaks at various wavenumbers, each corresponding to distinct functional groups in the molecule. The prominent peak at 3283 cm^{-1} represents O−H stretching vibrations, characteristic of hydroxyl groups. Peaks at 2924 cm^{-1} and 2853 cm^{-1} indicate C−H stretching from alkyl groups. The peak at 1704 cm^{-1} is attributed to C═O stretching, while the peak at 1605 cm^{-1} corresponds to aromatic C═C stretching. The peaks at 1455 cm^{-1} represent C−O stretching vibrations. Figure 5b displays the FTIR spectrum of the PVA and ascorbic acid mixture. The distinct peak at 3305 cm^{-1} represents O−H stretching vibrations due to the hydroxyl groups in both PVA and ascorbic acid. Peaks at 2933 cm^{-1} and 3084 cm^{-1} are associated with C−H stretching vibrations of the aliphatic groups. The peak at 1703 cm^{-1} and 1632 cm^{-1} indicates C═O stretching, in both PVA and ascorbic acid. Figure 5c illustrates the FTIR spectrum of the composite mixture containing PVA, ascorbic acid, and tannic acid. The peak at 3312 cm^{-1} represents O−H stretching, while the peaks at 3094 cm^{-1}, 2933 cm^{-1}, and 2815 cm^{-1} are associated with C−H stretching. The peak at 1707 cm^{-1} and 1635 cm^{-1} represents C═O stretching in two different molecules. One of the most noticeable changes is in the O−H stretching region (3200−3400 cm^{-1}). The broad peak in this region in Figure 5c (3312 cm^{-1}) appears to combine the O−H stretching vibrations from both tannic acid and PVA. This broadening and slight shift in the peak position indicates the formation of hydrogen bonds between the hydroxyl groups of tannic acid and PVA. Additionally, the C═O stretching vibration at around 1700 cm^{-1} shows a slight shift from 1704 cm^{-1} in tannic acid to 1707 cm^{-1} in the composite mixture. This slight shift could be due to the interaction between the carbonyl groups of tannic acid and the hydroxyl groups of PVA, possibly through hydrogen bonding. The presence of peaks at 1635 cm^{-1} and 1155 cm^{-1} in the composite spectrum suggests that some of the characteristic vibrations of both tannic acid and PVA are maintained in the mixture. However, the relative intensities and slight shifts in these peaks indicate that the chemical environment of these functional groups has been altered due to the interactions between the components.

3.7. The Effect of Ascorbic Acid Content on Water Evaporation of PVA/AS Blends. Water evaporation is a crucial parameter that determines hydrogel formulations' stability, shelf life, and performance, especially in biomedical applications where maintaining the desired moisture content is essential for proper functioning and compatibility with biological systems. Table 5 and Figure 6 present the water evaporation data for the PVA/AS blends irradiated at a dose of 7 kGy with varying ascorbic acid (AA) concentrations ranging

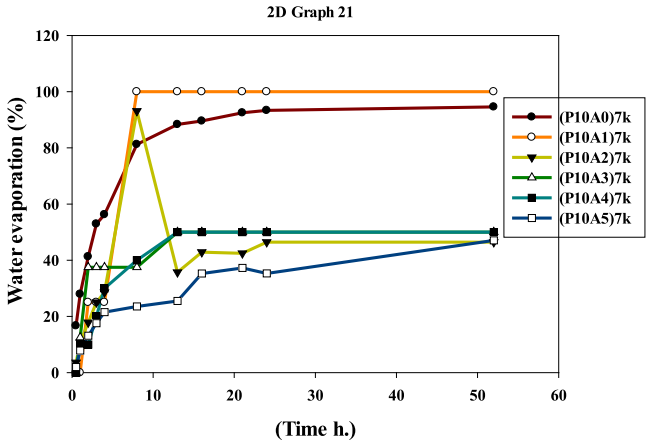

Figure 6. Effect of ascorbic acid content on water evaporation of PVA/AS blends.

from 0% to 5% w/w concerning PVA, over 52 h. The data shows that the water evaporation rate decreases with an increase in the concentration of ascorbic acid in the PVA/AS blends. The sample with 0% AA (P10A0)7k exhibits the highest water evaporation rate, with approximately 94.58% of the initial water content evaporating within 52 h. In contrast, the sample with 5% AA (P10A5)7k shows the lowest water evaporation rate, with only 47.06% of the initial water content evaporating simultaneously. This behavior can be attributed to the following factors: (1) ascorbic acid (AA) is a hygroscopic compound with a strong affinity for water molecules. The presence of AA in the PVA/AS blends enhances the water-retention capacity of the hydrogel, thereby reducing the rate of water evaporation. (2) AA may interact with the PVA chains through hydrogen bonding, forming a more tightly bound hydrogel network that restricts the mobility and evaporation of water molecules. (3) The addition of AA increases the ionic strength of the hydrogel system, which can lead to a higher degree of cross-linking or network formation during gamma irradiation. A more densely cross-linked network can better retain water molecules, resulting in a lower evaporation rate. (4) AA may also form a more hydrophilic environment within the hydrogel matrix, further enhancing water retention and reducing evaporation. The ability to modulate the water evaporation rate by varying the AA content is advantageous for tailoring the hydrogel formulations to specific biomedical applications. For instance, formulations with lower water evaporation rates may be desirable for wound dressings or drug delivery systems that require sustained moisture levels over extended periods. It is important to note that while a lower

https://doi.org/10.1021/acsomega.4c07119
ACS Omega 2025, 10, 13839−13853

Table 6. Effect of Irradiation Dose on Water Evaporation of PVA/AS Blends

sample	$(P_{10}A_2)_{0k}$	$(P_{10}A_2)_{3k}$	$(P_{10}A_2)_{7k}$	$(P_{10}A_2)_{9k}$	$(P_{10}A_2)_{12k}$	$(P_{10}A_2)_{15k}$
t.5	12%	25%	3.57%	9.5%	13.3%	3.5%
t1	20%	25%	10.71%	14%	20%	14.2%
t2	28%	25%	17.85%	19%	26.6%	14.3%
t3	36%	25%	25%	19%	33%	14.3%
t4	40%	100%	28.57%	28.5%	33%	25%
t8	44%	100%	93.2%	33.33%	33%	35.7%
t13	44%	100%	35.7%	38%	40%	39.2%
t16	52%	100%	42.85%	42.8%	53%	39.2%
t21	52%	100%	42.85%	47.6%	60%	39.2%
t24	52%	100%	46.42%	47.6%	60%	39.2%
t52	60%	100%	46.43%	52.38%	66.6%	50%

water evaporation rate is generally preferred for most biomedical applications, excessively low evaporation rates could lead to issues such as prolonged degradation times or potential microbial growth. Therefore, an optimal balance between water retention and evaporation should be achieved based on the specific requirements of the intended application. The water evaporation data should be analyzed with other properties, such as mechanical strength, swelling behavior, and bioadhesive performance, to develop a comprehensive understanding of the PVA/AS hydrogel formulations and optimize them accordingly.

3.8. The Effect of Irradiation Dose on Water Evaporation of PVA/AS Blends. The degree of cross-linking induced by gamma irradiation in PVA-based hydrogels is crucial in determining their water evaporation behavior. The extent of cross-linking, which is directly influenced by the irradiation dose, affects the hydrogel's network structure, porosity, and water-holding capacity, ultimately impacting the rate of water evaporation. Table 6 and Figure 7 present the

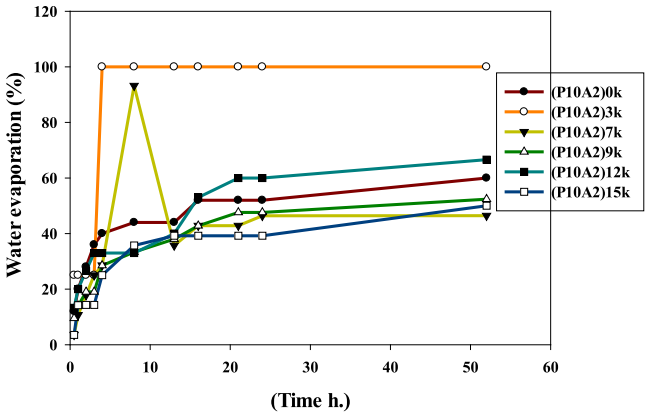

Figure 7. Effect of irradiation dose on water evaporation of PVA/AS blends.

water evaporation data for the PVA/AS blends containing 2% ascorbic acid (AA) and subjected to different gamma irradiation doses ranging from 0 kGy (nonirradiated) to 15 kGy, over 52 h. The data shows that the water evaporation rate generally increases with increasing irradiation dose, with some exceptions at lower doses. The nonirradiated sample (P10A2)0k exhibits a relatively low water evaporation rate, with approximately 60% of the initial water content evaporating within 52 h. This behavior can be attributed to the absence of cross-linking, resulting in a more linear or minimally branched polymer structure with a limited ability to retain water molecules effectively. As the irradiation dose increases to 3 kGy, the water evaporation rate remains unchanged, suggesting that the cross-linking process has not yet significantly influenced the water-holding capacity of the hydrogel at this dose level. However, as the irradiation dose increases further (7 kGy and beyond), a significant increase in the water evaporation rate is observed. This can be attributed to the following factors: (1) At higher irradiation doses, the cross-linking of PVA chains becomes more pronounced, forming a three-dimensional network structure with increased porosity and interconnected pores. (2) The increased porosity and pore interconnectivity facilitate the diffusion and evaporation of water molecules from the hydrogel matrix, resulting in a higher water evaporation rate. (3) The presence of ascorbic acid (AA) may contribute to the cross-linking process by generating free radicals and facilitating the formation of intermolecular and intramolecular cross-links between PVA chains, further enhancing the network formation and porosity. It is worth noting that beyond a certain irradiation dose (e.g., 12 kGy in this study), the water evaporation rate appears to plateau or decrease slightly (as observed for the 15 kGy sample). This behavior could be attributed to the following factors: (1) At very high irradiation doses, the degree of cross-linking may become excessive, leading to a more tightly bound and less porous network structure, which could hinder the diffusion and evaporation of water molecules. (2) Potential chain scission or degradation processes at very high irradiation doses may also contribute to the observed plateau or decrease in water evaporation rate. The ability to modulate the water evaporation rate by varying the irradiation dose is advantageous for tailoring the hydrogel formulations to specific biomedical applications. For instance, formulations with higher water evaporation rates may be desirable for applications that require rapid drying or moisture management, such as wound dressings or antiperspirants. Conversely, formulations with lower water evaporation rates could be beneficial for sustained drug delivery or applications requiring prolonged hydration. It is important to consider the water evaporation data with other properties, such as mechanical strength, swelling behavior, and bioadhesive performance, to optimize the formulation for the desired application while maintaining water retention and evaporation characteristics.

3.9. Microbial Contamination in PVA/AS Hydrogel Samples. Ensuring biomaterials' microbial safety and sterility, such as hydrogels intended for biomedical applications, is paramount. The presence of bacteria or fungi in these materials can pose serious health risks and compromise their

https://doi.org/10.1021/acsomega.4c07119
ACS Omega 2025, 10, 13839−13853

effectiveness. Table 7 and the accompanying figures provide valuable information on the microbial contamination levels in the different PVA/AS hydrogel samples prepared using gamma irradiation.

Table 7. Microbial Contamination in PVA/AS Hydrogel Samples

Sample	Fungal content	Bacterial content
(P10A0)0k	*Candida* + true fungi	X
(P10A1)0k	X	7 CFU/500 mL
(P10A2)0k	X	X
(P10A3)0k	2 types of fungi	X
(P10A4)0k	X	X
(P10A5)0k	X	X
(P10A0)3k	X	5 CFU/500 mL
(P10A1)3k	1 true fungi	X
(P10A2)3k	X	X
(P10A3)3k	X	1 CFU/500 mL
(P10A4)3k	X	X
(P10A5)3k	X	X
(P10A0)7k	X	X
(P10A1)7k	X	X
(P10A2)7k	X	X
(P10A3)7k	X	X
(P10A4)7k	1 CFU *Candida*	1 CFU/500 mL
(P10A5)7k	X	X
(P10A0)9k	X	X
(P10A1)9k	1 type fungi	X
(P10A2)9k	1 type fungi	X
(P10A3)9k	X	X
(P10A4)9k	X	1 CFU/500 mL
(P10A5)9k	X	X
(P10A0)12k	X	X
(P10A1)12k	1 CFU/500mL	1 CFU/500 mL
(P10A2)12k	X	X
(P10A3)12k	X	X
(P10A4)12k	X	X
(P10A5)12k	X	113 CFU/500 mL
(P10A0)15k	1 CFU/500 mL	1 CFU/500 mL
(P10A1)15k	X	X
(P10A2)15k	X	X
(P10A3)15k	X	X
(P10A4)15k	X	X
(P10A5)15k	X	X

The data in Table 7 represented a confirmation test to assess the presence or absence of bacterial and fungal contamination in the various PVA/AS hydrogel formulations prepared with different ascorbic acid (AA) concentrations (0−5%) and irradiation doses (0−15 kGy).

The data shows that most of the samples exhibit minimal or no microbial contamination, indicating the effectiveness of the gamma irradiation process in achieving microbial sterilization. However, a few samples show low bacterial or fungal contamination levels, which warrants further analysis and interpretation.

Several samples, such as (P10A1)0k, (P10A2)0k, (P10A3)7k, (P10A4)7k, (P10A5)7k, (P10A1)9k, (P10A2)9k, (P10A3)9k, (P10A4)15k, and (P10A5)15k, exhibit no detectable levels of bacterial or fungal contamination. This observation suggests that the combination of gamma irradiation and the antimicrobial properties of ascorbic acid effectively inhibited microbial growth in these formulations.

A few samples, such as (P10A0)3k, (P10A3)3k, (P10A4)9k, (P10A0)12k, and (P10A1)12k, show low levels of bacterial contamination, ranging from 1 to 7 CFU/500 mL (colony forming units per 500 mL). While these levels are relatively low, they indicate the presence of some bacterial species that may have survived the gamma irradiation process or potentially contaminated the samples during handling or testing.

Certain samples, such as (P10A0)0k, (P10A2)0k, (P10A3)0k, (P10A4)0k, (P10A0)7k, (P10A4)7k, (P10A0)9k, and (P10A1)9k, exhibit varying degrees of fungal contamination. The presence of fungi, including *Candida* and other species, is indicated in these samples. Fungi are generally more resistant to gamma irradiation than bacteria, which could explain their survival in some formulations. It is important to note that even at low levels, microbial contamination may not be acceptable for certain biomedical applications, especially those involving direct contact with tissues or the bloodstream. In such cases, additional sterilization measures or formulation modifications may be necessary to ensure complete microbial safety. The observed microbial contamination levels could be influenced by several factors, including: (1) effectiveness of gamma irradiation dose: Higher irradiation doses may be required to achieve complete sterilization, especially for more resistant microbial species or spores. (2) Influence of ascorbic acid concentration: ascorbic acid is known to possess antimicrobial properties, and higher concentrations may contribute to better microbial inhibition. (3) Sample handling and testing procedures: strict aseptic techniques and protocols should be followed during sample preparation, handling, and testing to minimize the risk of external contamination. (4) Inherent properties of the hydrogel formulation: factors such as pH, water content, and nutrient availability may influence the growth or survival of certain microbial species. To ensure the microbial safety of the PVA/AS hydrogel formulations, further optimization of the irradiation dose, ascorbic acid concentration, and sterilization procedures may be necessary. Additionally, incorporating antimicrobial agents or preservatives could be explored as an alternative or complementary approach to gamma irradiation. Conducting thorough microbial testing and validation studies ensures that the final hydrogel formulations meet the required safety standards and regulatory guidelines for their intended biomedical applications.

Figure 8 visually compares fungal growth across a series of Petri dishes organized into three rows. Each row contains dishes subjected to different conditions or treatments, showcasing varying degrees of fungal development, which is presumably the focus of a microbiological study or experiment. In Figure 8a there are five Petri dishes labeled as follows from left to right: $(P_{10}A_0)_0$k ("*Candida* + True Fungi"), $(P_{10}A_1)_3$k ("1 True Fungi"), $(P_{10}A_3)_0$k ("2 Types of Fungi"), $(P_{10}A_1)_9$k ("1 Type of Fungi"), and $(P_{10}A_2)_9$k ("1 Type of Fungi"). The first dish, $(P_{10}A_0)_0$k, exhibits the highest amount of visible fungal growth, which is extensive and likely includes a mix of *Candida* and other true fungi. Conversely, the dishes labeled $(P_{10}A_1)_3$k, $(P_{10}A_1)_9$k, and $(P_{10}A_2)_9$k show minimal fungal growth, indicating that the conditions in these dishes are less conducive to fungal proliferation. In Figure 8b, two larger Petri dishes, both labeled as 1CFU/500m, specifically $(P_{10}A_1)_{12}$k and $(P_{10}A_4)_9$k. These dishes show less visible fungal growth than those in the top row. The reduced growth in these dishes

https://doi.org/10.1021/acsomega.4c07119
ACS Omega 2025, 10, 13839−13853

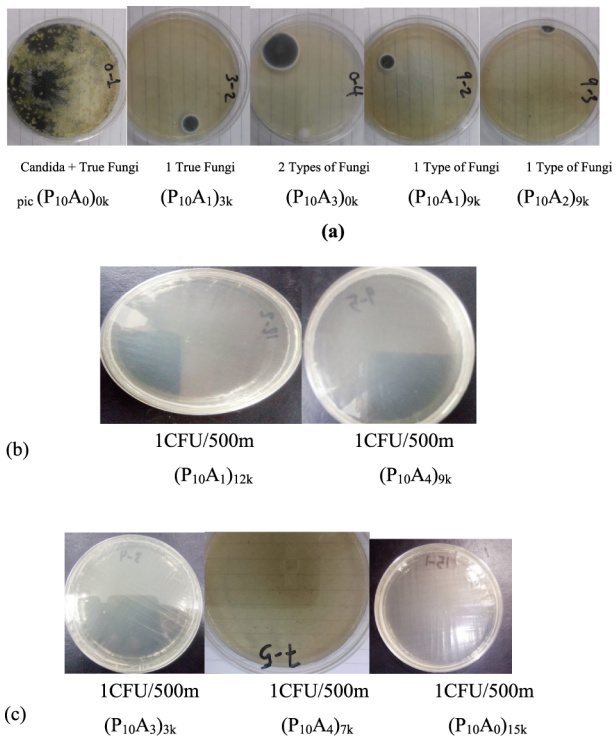

Figure 8. Comparison of fungal growth in PVA/AS hydrogel blends with varying ascorbic acid concentrations and gamma irradiation doses. (a) Fungal growth in samples $(P_{10}A_0)_0k$, $(P_{10}A_1)_3k$, $(P_{10}A_3)_0k$, $(P_{10}A_1)_9k$, and $(P_{10}A_2)_9k$. (b) Samples $(P_{10}A_1)_{12}k$ and $(P_{10}A_4)_9k$. (c) Samples $(P_{10}A_3)_3k$, $(P_{10}A_4)_7k$, and $(P_{10}A_0)_{15}k$. (CFU/500m = CFU/500 mL).

might be due to their specific treatment or the conditions provided, which were less favorable for extensive fungal development. The "1CFU/500m" label suggests a controlled, low-concentration inoculation meant to observe growth from a minimal starting population. In Figure 8c there are three more Petri dishes, also labeled as 1 CFU/500m: $(P_{10}A_3)_3k$, $(P_{10}A_4)_7k$, and $(P_{10}A_0)_{15}k$. The middle dish $(P_{10}A_4)_7k$ shows the most visible fungal growth in this row, indicating that it had conditions favorable for fungal development, despite the low initial inoculation. The other dishes in this row exhibit varying but generally lower levels of fungal growth. The lowest fungal growth is observed in dishes $(P_{10}A_1)_3k$, $(P_{10}A_1)_9k$, $(P_{10}A_2)_9k$, and $(P_{10}A_0)_{15}k$. These dishes display minimal visible fungal colonies on the agar surface, suggesting conditions that limit fungal proliferation. The highest fungal growth is noted in the dish $(P_{10}A_0)_0k$, labeled "*Candida* + True Fungi," which shows significant fungal growth covering much of the agar surface. This extensive growth suggests optimal conditions for the fungi present.

The visibility of fungal growth in these dishes highlights the differences in environmental conditions, treatment effects, or initial fungal populations, providing valuable insights into the factors influencing fungal proliferation in PVA/AS hydrogel formulations.

3.10. Antimicrobial Potential. Antimicrobial products have been used to prevent microbial illnesses that can lead to clinical poisoning over time.[31] Nonetheless, research into novel compounds for microbial suppression based on particular nanomaterials is gaining traction[32] This work used the well-agar diffusion technique to examine the antibacterial capability of the (P10A2)7k/TA as it was synthesized. According to our findings, the produced (P10A2)7k/TA (250 ppm) has a broad-spectrum deactivation impact on the examined bacteria. Furthermore, as Table 8 illustrates, (P10A2)7k/TA (250 ppm) had the strongest effect against all tested microbes.

Table 8. Inhibition Zones and MICs of Bimetallic (P10A2)7k/TA against Bacterial and Fungal Strains

		(P10A2)7k/TA		
Bacterial strain	DMSO IZ (mm)	IZ (mm)	MIC (μg/mL)[a]	CD or NS IZ (mm)
Pseudomonas aeruginosa	ND	15.5 ± 1.5[e]	250	ND
Klebsiella pneumoniae	ND	13.0 ± 1.3[f]	500	ND
Escherichia coli	ND	19.5 ± 1.6[b]	62.5	ND
Staphylococcus aureus	ND	21.5 ± 0.7[a]	31.25	ND
Staphylococcus epidermidis	ND	13.5 ± 1.5[e,f]	500	ND
Bacillus subtilis	ND	18.5 ± 0.7[c]	62.5	ND
Candida albicans	ND	17.5 ± 1.8[d]	125	ND
Candida tropicalis	ND	15.5 ± 1.6[e]	250	ND

[a]Values are means ± SD (n = 3). Data within the groups were analyzed using one-way analysis of variance (ANOVA) followed by a,b,c,d,e,f Duncan's multiple range test (DMRT).

3.10.1. MIC Starting with 1000 (μg/mL). The results demonstrated that the examined microorganisms were robust to the utilized medicines and that our specimens were stronger than the standard antibiotics. The as-synthesized (P10A2)7k/TA antimicrobial qualities were evaluated using a common antibiotic such as Amoxycillin (CD), and the outcomes showed these conclusions. Several characteristics, including a tiny size and an elevated surface-to-volume ratio, are common in the synthesized samples. They can display distinct and important behaviors when incorporating and connecting with some infectious microbes, such as bacteria.[33] The minimum inhibition concentration (MIC) values for all investigated microorganisms in the integrated samples varied from 31.25 to 500 μg/mL. (P10A2)7k/TA demonstrated a promising MIC of 31.25 μg/mL against *S. aureus* (Table 7).

The created (P10A2)7k/TA's encouraging attributes are crucial to their antibacterial capabilities; the generated nanocomposites' elemental structure, purity, and size should be examined to understand their antimicrobial activities.[34] The exceptional antibacterial efficacy and the produced (P10A2)7k/TA characteristics are significant. The produced (P10A2)7k/TA's antibacterial activity against all existing bacteria was enhanced by the (P10A2)7k/TA and its promising particle size, even at extremely low concentrations (31.25 μg/mL). Beyond the typical organic and artificial antimicrobial agents, they retained the appropriate physical and chemical properties, such as a more unique connection for interactions, allowing for higher synergy with more harmful bacteria and yeast and enhancing their antibacterial efficacy.[35]

However, it is unknown how nanosilica works as an antibacterial. Amazingly sophisticated processes existed, such as the dispersion of reactive oxygen species (ROS) (superoxide anion; O_2^-).[36] The pathogenic bacteria's combination of (P10A2)7k/TA and an alkaline inclination was used to illustrate the antimicrobial activity mechanism.[37] According to certain theories, (P10A2)7k/TA may modify the shape and content of microbial films, modify the permeability of

https://doi.org/10.1021/acsomega.4c07119
ACS Omega 2025, 10, 13839−13853

microbial membranes, and induce oxidative stress genes to reside in response to H_2O_2 generation.[38]

3.11. Antibiofilm Activity of (P10A2)7k/TA. It has been established that pathogenic microorganisms with exopolysaccharide (EPS) secretion exhibit biofilm formation.[39] Six bacterial species were used to evaluate the biofilm eradication activity of (P10A2)7k/TA. According to the results, most of the tested strains' ability to produce biofilm was inhibited by (P10A2)7k/TA. The antibiofilm effectiveness of (P10A2)7k/TA versus the strains isolated were displayed in Table 9. It is important to note that research was done on (P10A2)7k/TA to prevent biofilm formation during the initial stage of antimicrobial action, known as continuous adhesion. The potential of antimicrobial agents, the tested (P10A2)7k/TA's large surface area, physical properties like particle size and invasion abilities, and additional chemical factors that affect the nanocomposite's interaction with biofilm-producing microbes, such as surface charge, all influence the inhibitory percentage.[40]

Table 9. Semi-Quantitative Inhibition % of the Biofilm Formation for Non-Treated and Treated Bacterial Pathogens with (P10A2)7k/TA[a]

Bacterial isolate	O.D. of control	O.D. after treatment	Inhibition %
Pseudomonas aeruginosa	$0.943^{b} \pm 0.023$	$0.400^{b} \pm 0.034$	57.5
Klebsiella pneumoniae	$0.801^{f} \pm 0.011$	$0.385^{d} \pm 0.012$	51.9
Escherichia coli	$0.923^{c} \pm 0.040$	$0.345^{e} \pm 0.022$	62.6
Staphylococcus aureus	$0.872^{e} \pm 0.015$	$0.222^{f} \pm 0.058$	74.5
Staphylococcus epidermidis	$0.551^{g} \pm 0.010$	$0.210^{g} \pm 0.010$	61.8
Bacillus subtilis	$0.790^{g} \pm 0.013$	$0.390^{e} \pm 0.050$	50.6
Candida albicans	$0.888^{d} \pm 0.013$	$0.321^{e} \pm 0.050$	63.3
Candida tropicalis	$0.990^{a} \pm 0.013$	$0.543^{a} \pm 0.050$	45.1

[a]Values are means ± SD (n = 3). Data within the groups are analyzed using one-way analysis of variance (ANOVA) followed by a,b,c,d,e,f,g,h Duncan's multiple range test (DMRT).

The antibiofilm activity of (P10A2)7k/TA toward *S. aureus* (74.50%), *C. albicans* (63.3%), and *E. coli* (62.6%) was maximum at a concentration of 250 ppm. Using (P10A2)7k/TA as biofilm suppressive agents has been shown to include two steps. Microbial cells' adherence to the hard substrate may be compromised in the early stages. Therefore, it may be possible to prevent EPS production and the development of the mature stage. In the second step, the active sample can continue to affect the developed biofilm by penetrating the film and killing the microbial cells, which causes the created biofilm to disperse. In light of this, we believe that green sample-based antibiofilm coatings are potential probes for biofilm visualization, therapy, and eradication. Other benefits include their broad range efficacy and low toxicity. Therefore, green samples might provide visual monitoring and detect the inhibitory process.[41]

3.12. Growth Curve Method: Kinetic Study. Figure 9 shows the impact of (P10A2)7k/TA on *S. aureus* growth. In the control sample, *S. aureus* overgrew, reaching its highest optical density at λ = 600 nm (OD_{600}) value at 3.33 nm. Indifference, (P10A2)7k/TA's OD_{600} value (1.23 nm) revealed the poorest results, indicating the influence of repression on *S. aureus* growth. The production of certain ROS on the outer layer of the synthesized samples has frequently been reported in earlier research.[42] ROS produced by (P10A2)7k/TA can kill bacteria by causing lipid peroxidation, DNA damage, and protein oxidation.[43] Furthermore, although the *S. aureus* membrane retains a negative charge, the metal ions produced by (P10A2)7k/TA have a positive charge. This indicates arise in response to halting bacterial DNA replication, protein denaturation, and bacterial cell disintegration.[44] The increased sensitivity of Gram-positive bacteria to the produced (P10A2)7k/TA may be due to their membranes' increased rigidity.[45]

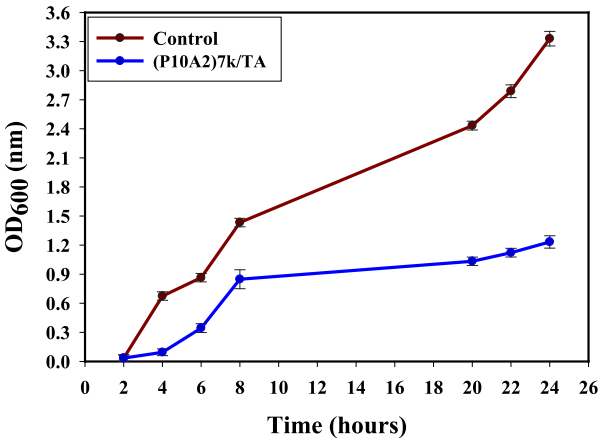

Figure 9. Effect of (P10A2)7k/TA on the growth curve of *S. aureus*.

Other factors that could make it easier for irradiated nanosilicas to attach themselves to Gram-positive bacteria include their size, shape, and surface charge. According to Xu et al.[46] some produced NPs broke the *E. coli* membrane after 80 min of UV irradiation. suggesting that disinfection had finished. Several investigations revealed that most NPs have antibacterial ability against various bacterial strains, such as *S. aureus* and *E. coli*.[47]

3.12.1. Bacterial Protein Leakage Investigation. The Bradford technique calculated the proteins released from the treated *S. aureus* solution.[48] As shown in Figure 10, the quantity of bacterial protein eliminated is directly related to the concentration of (P10A2)7k/TA (at different concentrations). After treatment with (P10A2)7k/TA, at a concentration of 1.0

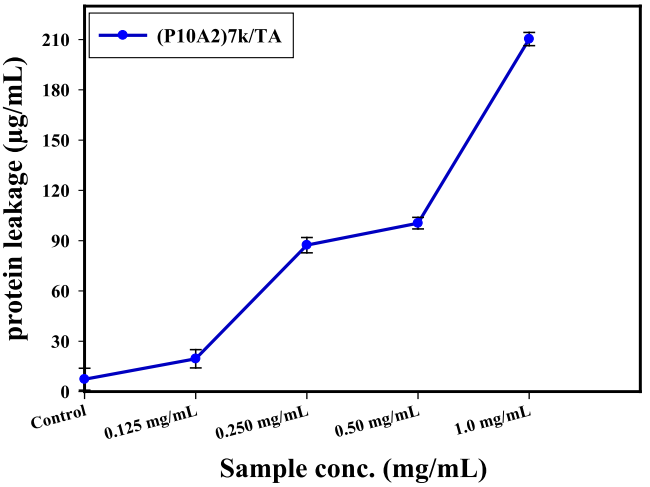

Figure 10. Shows the effect of (P10A2)7k/TA on protein leakage from *S. aureus* cell membranes.

https://doi.org/10.1021/acsomega.4c07119
ACS Omega 2025, 10, 13839−13853

mg/mL, the amount of bacterial protein removed is counted to be 210.34 μg/mL. This indicates the antibacterial properties of the synthesized (P10A2)7k/TA and explains the appearance of holes in the *S. aureus* membrane that aid in releasing proteins from the cytoplasm of the bacteria.

The results showed that raising the concentration of improved *S. aureus* permeability in the membrane leads to a direct proportionate removal of bacterial protein. The primary factor suppressing the bacterial bulk is the favorable influence on membrane permeability concerning protein leakage. Similar findings were defined when combining NPs in corresponding investigations like [40] and [41], which indicated concentration-dependency for the dislodgment in the bacterial barrier and indicated bacterial internal organelle leaking through the extracellular cell structure.

Paul et al.[49] state that the rate variation between the associated electric conductivity established the difference in the permeability of the bacterial membrane. One of the most important methods for assessing the structural strength of any microorganism is the protein leakage test. Leakage eventually turned into regular microbial damage, and the discharge of cell components resulted in cell death.

4. CONCLUSION

In this study, we successfully developed a novel (PVA/AS)/TA hydrogel with enhanced bioadhesive, mechanical, and antimicrobial properties through gamma irradiation. Incorporating 5 wt % TA significantly improved the lap shear strength, tensile strength, and elongation at break, demonstrating the hydrogel's robust mechanical performance. The (P10A2)7k/TA hydrogel exhibited potent antimicrobial activity against various bacterial and fungal strains, highlighting its potential for preventing infections in biomedical applications. The ability to modulate the viscosity and water evaporation rates by varying the AA content and irradiation dose allows for the customization of hydrogel properties to suit specific applications. The synergistic effects of gamma irradiation and TA modification resulted in a hydrogel formulation with promising applications in wound healing, drug delivery, and tissue engineering. The inclusion of TA in PVA/AS hydrogels significantly enhances the mechanical properties and bioadhesive strength through various intermolecular interactions. The detailed mechanical properties presented in Table 4 provide valuable insights into the performance of the (PVA/AS)/TA hydrogels, aiding in selecting optimal formulations for different biomedical applications. The ability to tailor the mechanical properties through TA modification and irradiation doses enhances the versatility and applicability of the hydrogels in diverse biomedical contexts. Incorporating TA may also impart additional functionalities, such as antioxidant and antimicrobial properties, further enhancing the potential biomedical applications of the (PVA/AS)/TA hydrogel formulation.

AUTHOR INFORMATION

Corresponding Author

Mohamed Mohamady Ghobashy − *Radiation Research of Polymer Chemistry Department, National Center for Radiation Research and Technology (NCRRT), Egyptian Atomic Energy Authority, Cairo, Nasr City 2980, Egypt;* orcid.org/0000-0003-0968-1423; Email: Mohamed_ghobashy@yahoo.com

Authors

Shreen Adel Rashiq − *Department of Chemistry, Faculty of Science, Ain Shams University, Cairo, Abbassiya 11566, Egypt*

Nour E. A. Abd El-Sattar − *Department of Chemistry, Faculty of Science, Ain Shams University, Cairo, Abbassiya 11566, Egypt; Basic & Medical Sciences Department, Faculty of Dentistry, Alryada University for Science & Technology, Sadat City 32897, Egypt;* orcid.org/0000-0001-6680-4448

Hoda Abd Elhay abd Elhamid − *Department of Chemistry, Faculty of Science, Ain Shams University, Cairo, Abbassiya 11566, Egypt*

Gharieb S. El-Sayyad − *Medical Laboratory Technology Department, Faculty of Applied Health Sciences Technology, Badr University in Cairo (BUC), Cairo, Badr City 11829, Egypt; Drug Microbiology Lab., Drug Radiation Research Department, National Center for Radiation Research and Technology (NCRRT), Egyptian Atomic Energy Authority (EAEA), Cairo 2980, Egypt*

Ghada Bassioni − *Chemistry Department, Faculty of Engineering, Ain Shams University, Cairo 11517, Egypt;* orcid.org/0000-0001-8928-6428

Complete contact information is available at: https://pubs.acs.org/10.1021/acsomega.4c07119

Notes

The authors declare no competing financial interest.

ACKNOWLEDGMENTS

The authors would like to express their gratitude to the central lab at the National Center for Radiation Research and Technology (NCRRT), Egyptian Atomic Energy Authority for their technical assistance and valuable contributions to this research.

REFERENCES

(1) Xiong, Y.; Zhang, X.; Ma, X.; Wang, W.; Yan, F.; Zhao, X.; Chu, X.; Xu, W.; Sun, C. A review of the properties and applications of bioadhesive hydrogels. *Polym. Chem.* **2021**, *12* (26), 3721−3739.

(2) Moroni, L.; Elisseeff, J. H. Biomaterials engineered for integration. *Mater. Today* **2008**, *11* (5), 44−51.

(3) Ghani, S. A. A.; El-Sayed, A. A. M.; Ibrahim, M. I. A.; Ghobashy, M. M.; Shreadah, M. A.; Shabaka, S. Characterization and distribution of plastic particles along Alexandria beaches, Mediterranean Coast of Egypt, using microscopy and thermal analysis techniques. *Sci. Total Environ.* **2022**, *834*, 155363.

(4) El-Sayed, A. A. M.; Ibrahim, M. I. A.; Shabaka, S.; Ghobashy, M. M.; Shreadah, M. A.; Ghani, S. A. A. Microplastics contamination in commercial fish from Alexandria City, the Mediterranean Coast of Egypt. *Environ. Pollut.* **2022**, *313*, 120044.

(5) Ghobashy, M. M.; Elbarbary, A. M.; Hegazy, D. E.; Maziad, N. A. Radiation synthesis of pH-sensitive 2-(dimethylamino) ethyl methacrylate/polyethylene oxide/ZnS nanocomposite hydrogel membrane for wound dressing application. *J. Drug Delivery Sci. Technol.* **2022**, *73*, 103399.

(6) Abd El-Sattar, N. E. A.; El-Hddad, S. E. S. A.; Ghobashy, M. M.; Zaher, A. A.; El-Adl, K. Nanogel-mediated drug delivery system for anticancer agent: pH stimuli responsive poly (ethylene glycol/acrylic acid) nanogel prepared by gamma irradiation. *Bioorg. Chem.* **2022**, *127*, 105972.

(7) Alkhursani, S. A.; Ghobashy, M. M.; Al-Gahtany, S. A.; Meganid, A. S.; Abd El-Halim, S. M.; Ahmad, Z.; Khan, F. S.; Atia, G. A. N.; Cavalu, S. Application of nano-inspired scaffolds-based biopolymer

hydrogel for bone and periodontal tissue regeneration. *Polymers* **2022**, *14* (18), 3791.
(8) Ghobashy, M. M.; Mousaa, I. M.; El-Sayyad, G. S. Radiation synthesis of urea/hydrogel core shells coated with three different natural oils via a layer-by-layer approach: An investigation of their slow release and effects on plant growth-promoting rhizobacteria. *Prog. Org. Coat.* **2021**, *151*, 106022.
(9) Peppas, N. A.; Sahlin, J. J. Hydrogels as mucoadhesive and bioadhesive materials: a review. *Biomaterials* **1996**, *17* (16), 1553−1561.
(10) Knuth, K.; Amiji, M.; Robinson, J. R. Hydrogel delivery systems for vaginal and oral applications: Formulation and biological considerations. *Adv. Drug Delivery Rev.* **1993**, *11* (1−2), 137−167.
(11) Bu, Y.; Pandit, A. Cohesion mechanisms for bioadhesives. *Bioact. Mater.* **2022**, *13*, 105−118.
(12) Varghese, S. A.; Rangappa, S. M.; Siengchin, S.; Parameswaranpillai, J. Natural polymers and the hydrogels prepared from them. In *Hydrogels based on natural polymers*; Elsevier, 2020; pp. 17−47.
(13) Bal-Ozturk, A.; Cecen, B.; Avci-Adali, M.; Topkaya, S. N.; Alarcin, E.; Yasayan, G.; Li, Y.-C. E.; Bulkurcuoglu, B.; Akpek, A.; Avci, H.; et al. Tissue adhesives: From research to clinical translation. *Nano Today* **2021**, *36*, 101049.
(14) Pourshahrestani, S.; Zeimaran, E.; Kadri, N. A.; Mutlu, N.; Boccaccini, A. R. Polymeric hydrogel systems as emerging biomaterial platforms to enable hemostasis and wound healing. *Adv. Healthcare Mater.* **2020**, *9* (20), 2000905.
(15) Fuchs, S.; Shariati, K.; Ma, M. Specialty tough hydrogels and their biomedical applications. *Adv. Healthcare Mater.* **2020**, *9* (2), 1901396.
(16) Jafari, H.; Ghaffari-Bohlouli, P.; Niknezhad, S. V.; Abedi, A.; Izadifar, Z.; Mohammadinejad, R.; Varma, R. S.; Shavandi, A. Tannic acid: a versatile polyphenol for design of biomedical hydrogels. *J. Mater. Chem. B* **2022**, *10* (31), 5873−5912.
(17) Chen, Y.-N.; Jiao, C.; Zhao, Y.; Zhang, J.; Wang, H. Self-assembled polyvinyl alcohol−tannic acid hydrogels with diverse microstructures and good mechanical properties. *ACS Omega* **2018**, *3* (9), 11788−11795.
(18) Hong, K. H. Preparation and properties of polyvinyl alcohol/tannic acid composite film for topical treatment application. *Fibers Polym.* **2016**, *17*, 1963−1968.
(19) Hakimi, F.; Sharifyrad, M.; Safari, H.; Khanmohammadi, A.; Gohari, S.; Ramazani, A. Amygdalin/chitosan-polyvinyl alcohol/cerium-tannic acid hydrogel as biodegradable long-time implant for cancer recurrence care applications: An in vitro study. *Heliyon* **2023**, *9* (11), No. e21835.
(20) Ahankari, S.; Lasrado, D.; Subramaniam, R. Advances in materials and fabrication of separators in supercapacitors. *Mater. Adv.* **2022**, *3* (3), 1472−1496.
(21) Sultan, A. S.; Vila, T.; Hefni, E.; Karlsson, A. J.; Jabra-Rizk, M. A. Evaluation of the antifungal and wound-healing properties of a novel peptide-based bioadhesive hydrogel formulation. *Antimicrob. Agents Chemother.* **2019**, *63* (10), 10−128.
(22) Komara, I.; Susanto, A.; Amaliya, A.; Abbas, B.; Warastuti, Y.; Hendiani, I.; Miranda, A.; Erliani, A. P. The effect of gamma-ray irradiation on the physical, mechanical, and morphological characteristics of PVA-collagen-chitosan as a guided tissue regeneration (GTR) membrane material. *Euro. J. Dentistry* **2023**, *17* (2), 530−538.
(23) Demeter, M.; Scărişoreanu, A.; Călina, I. State of the art of hydrogel wound dressings developed by ionizing radiation. *Gels* **2023**, *9*, 55.
(24) Standards, N. C. f. C. L. *Reference method for broth dilution antifungal susceptibility testing of yeasts*; National Committee for Clinical Laboratory Standards: Wayne, PA, 2002.
(25) (a) Valgas, C.; Souza, S. M. D.; Smânia, E.; Smânia, A. Screening methods to determine antibacterial activity of natural products. *Braz. J. Microbiol.* **2007**, *38*, 369−380. (b) Hashem, A. H.; Khalil, A. M. A.; Reyad, A. M.; Salem, S. S. Biomedical Applications of Mycosynthesized Selenium Nanoparticles Using Penicillium expansum ATTC 36200. *Biol. Trace Elem. Res.* **2021**, 1−11. (c) Hashem, A. H.; Shehabeldine, A. M.; Abdelaziz, A. M.; Amin, B. H.; Sharaf, M. H. Antifungal Activity of Endophytic Aspergillus terreus Extract Against Some Fungi Causing Mucormycosis: Ultrastructural Study. *Appl. Biochem. Biotechnol.* **2022**, *194*, 3468.
(26) Christensen, G. D.; Simpson, W. A.; Bisno, A. L.; Beachey, E. H. Adherence of slime-producing strains of Staphylococcus epidermidis to smooth surfaces. *Infect. Immun.* **1982**, *37* (1), 318−326.
(27) Ansari, M. A.; Khan, H. M.; Khan, A. A.; Cameotra, S. S.; Pal, R. Antibiofilm efficacy of silver nanoparticles against biofilm of extended spectrum β-lactamase isolates of *Escherichia coli* and Klebsiella pneumoniae. *Appl. Nanosci.* **2014**, *4*, 859−868.
(28) Huang, W.; Wang, J.-Q.; Song, H.-Y.; Zhang, Q.; Liu, G.-F. Chemical analysis and in vitro antimicrobial effects and mechanism of action of Trachyspermum copticum essential oil against *Escherichia coli*. *Asian Pacific J. Tropical Med.* **2017**, *10* (7), 663−669.
(29) Agarwal, H.; Nakara, A.; Menon, S.; Shanmugam, V. Eco-friendly synthesis of zinc oxide nanoparticles using Cinnamomum Tamala leaf extract and its promising effect towards the antibacterial activity. *J. Drug Delivery Sci. Technol.* **2019**, *53*, 101212.
(30) Brownlee, K.; Finney, D. J.; Tattersfield, F. Probit Analysis: A Statistical Treatment of the Sigmoid Response Curve. *JSTOR* **1952**, *47* (260), 687.
(31) Prabhu, S.; Poulose, E. K. Silver nanoparticles: mechanism of antimicrobial action, synthesis, medical applications, and toxicity effects. *Int. Nano Lett.* **2012**, *2*, 32.
(32) Fatehbasharzad, P.; Fatehbasharzad, P.; Sillanpää, M.; Shamsi, Z. Investigation of bioimpacts of metallic and metallic oxide nanostructured materials: size, shape, chemical composition, and surface functionality: a review. *Part Part Syst. Charact.* **2021**, *38* (10), 2100112.
(33) Palencia, S. L.; Buelvas, A. M.; Palencia, M. S. Interaction mechanisms of inorganic nanoparticles and biomolecular systems of microorganisms. *Curr. Chem. Biol.* **2015**, *9* (1), 10−22.
(34) El-Sayyad, G. S.; Elfadil, D.; Gaballah, M. S.; El-Sherif, D. M.; Abouzid, M.; Nada, H. G.; Khalil, M. S.; Ghorab, M. A. Implication of nanotechnology to reduce the environmental risks of waste associated with the COVID-19 pandemic. *RSC Adv.* **2023**, *13* (18), 12438−12454.
(35) Hashem, A. H.; Saied, E.; Ali, O. M.; Selim, S.; Al Jaouni, S. K.; Elkady, F. M.; El-Sayyad, G. S. Pomegranate Peel Extract Stabilized Selenium Nanoparticles Synthesis: Promising Antimicrobial Potential, Antioxidant Activity, Biocompatibility, and Hemocompatibility. *Appl. Biochem. Biotechnol.* **2023**, *195*, 5753.
(36) Dryden, M. Reactive oxygen species: a novel antimicrobial. *Int. J. Antimicrob. Agents* **2018**, *51* (3), 299−303.
(37) Hashem, A. H.; El-Sayyad, G. S. Antimicrobial and anticancer activities of biosynthesized bimetallic silver-zinc oxide nanoparticles (Ag-ZnO NPs) using pomegranate peel extract. *Biomass Convers. Biorefin.* **2024**, *14*, 20345.
(38) Abdel Maksoud, M. I. A.; El-Sayyad, G. S.; El-Bastawisy, H. S.; Fathy, R. M. Antibacterial and antibiofilm activities of silver-decorated zinc ferrite nanoparticles synthesized by a gamma irradiation-coupled sol−gel method against some pathogenic bacteria from medical operating room surfaces. *RSC Adv.* **2021**, *11* (45), 28361−28374.
(39) Atkin, K. E.; MacDonald, S. J.; Brentnall, A. S.; Potts, J. R.; Thomas, G. H. A different path: revealing the function of staphylococcal proteins in biofilm formation. *FEBS Lett.* **2014**, *588* (10), 1869−1872.
(40) Abd Elkodous, M.; El-Sayyad, G. S.; Abdelrahman, I. Y.; El-Bastawisy, H. S.; Mohamed, A. E.; Mosallam, F. M.; Nasser, H. A.; Gobara, M.; Baraka, M. A.; Elsayed, M. A.; El-Batal, A. I. Therapeutic and diagnostic potential of nanomaterials for enhanced biomedical applications. *Colloids Surf., B* **2019**, *180*, 411−428.
(41) Priyadarshini, E.; Rawat, K.; Bohidar, H. B. Quantum Dots-Based Nano-Coatings for Inhibition of Microbial Biofilms: a Mini Review. In *Nonmagnetic and Magnetic Quantum Dots*; IntechOpen, 2017.

https://doi.org/10.1021/acsomega.4c07119
ACS Omega 2025, 10, 13839−13853

(42) (a) Fathy, R. M.; Mahfouz, A. Y. Eco-friendly graphene oxide-based magnesium oxide nanocomposite synthesis using fungal fermented by-products and gamma rays for outstanding antimicrobial, antioxidant, and anticancer activities. *J. Nanostruct. Chem.* **2021**, *11*, 301. (b) Joe, A.; Park, S.-H.; Kim, D.-J.; Lee, Y.-J.; Jhee, K.-H.; Sohn, Y.; Jang, E.-S. Antimicrobial activity of ZnO nanoplates and its Ag nanocomposites: Insight into an ROS-mediated antibacterial mechanism under UV light. *J. Solid State Chem.* **2018**, *267*, 124−133.
(43) Naik, M. M.; Naik, H. B.; Nagaraju, G.; Vinuth, M.; Naika, H. R.; Vinu, K. Green synthesis of zinc ferrite nanoparticles in Limonia acidissima juice: characterization and their application as photocatalytic and antibacterial activities. *Microchem. J.* **2019**, *146*, 1227−1235.
(44) Sharmila, G.; Thirumarimurugan, M.; Muthukumaran, C. Green synthesis of ZnO nanoparticles using Tecoma castanifolia leaf extract: characterization and evaluation of its antioxidant, bactericidal and anticancer activities. *Microchem. J.* **2019**, *145*, 578−587.
(45) Samavati, A.; Mustafa, M.; Ismail, A.; Othman, M.; Rahman, M. Copper-substituted cobalt ferrite nanoparticles: structural, optical and antibacterial properties. *Mater. Express* **2016**, *6* (6), 473−482.
(46) Xu, Y.; Liu, Q.; Xie, M.; Huang, S.; He, M.; Huang, L.; Xu, H.; Li, H. Synthesis of zinc ferrite/silver iodide composite with enhanced photocatalytic antibacterial and pollutant degradation ability. *J. Colloid Interface Sci.* **2018**, *528*, 70−81.
(47) (a) Patil, S.; Naik, H. S.; Nagaraju, G.; Viswanath, R.; Rashmi, S.; Vijay Kumar, M. Sugarcane juice mediated eco-friendly synthesis of visible light active zinc ferrite nanoparticles: Application to degradation of mixed dyes and antibacterial activities. *Mater. Chem. Phys.* **2018**, *212*, 351−362. (b) Ashour, A.; El-Batal, A. I.; Maksoud, M. A.; El-Sayyad, G. S.; Labib, S.; Abdeltwab, E.; El-Okr, M. Antimicrobial activity of metal-substituted cobalt ferrite nanoparticles synthesized by sol−gel technique. *Particuology* **2018**, *40*, 141−151. (c) Maksoud, M. A.; El-Sayyad, G. S.; Ashour, A.; El-Batal, A. I.; Abd-Elmonem, M. S.; Hendawy, H. A.; Abdel-Khalek, E.; Labib, S.; Abdeltwab, E.; El-Okr, M. Synthesis and characterization of metals-substituted cobalt ferrite [Mx Co (1-x) Fe2O4;(M= Zn, Cu and Mn; x= 0 and 0.5)] nanoparticles as antimicrobial agents and sensors for Anagrelide determination in biological samples. *Mater. Sci. Eng. C Mater. Biol. Appl.* **2018**, *92*, 644−656. (d) Maksoud, M. A.; El-Sayyad, G. S.; Ashour, A.; El-Batal, A. I.; Elsayed, M. A.; Gobara, M.; El-Khawaga, A. M.; Abdel-Khalek, E.; El-Okr, M. Antibacterial, antibiofilm, and photocatalytic activities of metals-substituted spinel cobalt ferrite nanoparticles. *Microb. Pathog.* **2019**, *127*, 144−158. (e) Maksoud, M. A.; El-Sayyad, G. S.; Abokhadra, A.; Soliman, L.; El-Bahnasawy, H.; Ashour, A. Influence of Mg 2+ substitution on structural, optical, magnetic, and antimicrobial properties of Mn−Zn ferrite nanoparticles. *J. Mater. Sci.: Mater. Electron.* **2020**, *31* (3), 2598−2616. (f) Maksoud, M. I. A. A.; El-Sayyad, G. S.; El-Khawaga, A. M.; Abd Elkodous, M.; Abokhadra, A.; Elsayed, M. A.; Gobara, M.; Soliman, L.; El-Bahnasawy, H.; Ashour, A. Nanostructured Mg substituted Mn-Zn ferrites: A magnetic recyclable catalyst for outstanding photocatalytic and antimicrobial potentials. *J. Hazard. Mater.* **2020**, *399*, 123000. (g) El-Sayyad, G. S.; Abd Elkodous, M.; El-Khawaga, A. M.; Elsayed, M. A.; El-Batal, A. I.; Gobara, M. Merits of photocatalytic and antimicrobial applications of gamma-irradiated Co x Ni 1− x Fe 2 O 4/SiO 2/TiO 2; x= 0.9 nanocomposite for pyridine removal and pathogenic bacteria/fungi disinfection: implication for wastewater treatment. *RSC Adv.* **2020**, *10* (9), 5241−5259. (h) Abd Elkodous, M.; El-Sayyad, G. S.; Youssry, S. M.; Nada, H. G.; Gobara, M.; Elsayed, M. A.; El-Khawaga, A. M.; Kawamura, G.; Tan, W. K.; El-Batal, A. I.; et al. Carbon-dot-loaded Co x Ni 1− x Fe 2 O 4; x= 0.9/SiO 2/TiO 2 nanocomposite with enhanced photocatalytic and antimicrobial potential: An engineered nanocomposite for wastewater treatment. *Sci. Rep.* **2020**, *10* (1), 11534. (i) Abd Elkodous, M.; El-Sayyad, G. S.; Maksoud, M. A.; Kumar, R.; Maegawa, K.; Kawamura, G.; Tan, W. K.; Matsuda, A. Nanocomposite matrix conjugated with carbon nanomaterials for photocatalytic wastewater treatment. *J. Hazard. Mater.* **2021**, *410*, 124657.
(48) Bradford, M. M. A rapid and sensitive method for the quantitation of microgram quantities of protein utilizing the principle of protein-dye binding. *Anal. Biochem.* **1976**, *72* (1−2), 248−254.
(49) Paul, D.; Maiti, S.; Sethi, D. P.; Neogi, S. Bi-functional NiO-ZnO nanocomposite: Synthesis, characterization, antibacterial and photo assisted degradation study. *Adv. Powder Technol.* **2021**, *32* (1), 131−143.

https://doi.org/10.1021/acsomega.4c07119
ACS Omega 2025, 10, 13839−13853